

Actuators for Dielectric Barrier Discharge Reactor Used in Synthesis of Metal Nanoparticles

Nikola Bednar, Goran Stojanović
Faculty of Technical Sciences
University of Novi Sad
Novi Sad, Serbia
bednar@uns.ac.rs, sgoran@uns.ac.rs

Jovan Matović
Institute of Sensor and Actuator Systems
Vienna University of Technology
Vienna, Austria
Jovan.Matovic@tuwien.ac.at

Abstract—In this paper we present a plasma reactor based on surface dielectric barrier discharges. This apparatus can be used in the process of metal nanoparticle synthesis as a source of reactive ions which take a part in reduction of metallic salts in order to produce atomic metal clusters. Four different plasma actuators have been fabricated and their electrical, thermal and optical properties are compared and presented.

Keywords—dielectric barrier discharge; electrodes; non-thermal plasma; metal nanoparticles; characterization.

I. INTRODUCTION

In recent years much attention has been given to dielectric barrier discharges (DBDs) due to its generation of non-equilibrium plasma in an economic and reliable way. This has led to a number of important applications including industrial ozone generation, surface modification of polymers, plasma-chemical vapor deposition, pollution control, excitation of CO₂ lasers, excimer lamps, air-flow control, nanoparticle synthesis, and large-area flat plasma-display panels [1-4].

There are several papers in which DBD plasma actuators were used for synthesis of metallic nanoparticles [5-11]. All of them utilize volume DBD configurations in the form of plasma jets, which deliver reactive species only to small surfaces (few mm²). However, in order to distribute created ions over the much larger areas, surface DBDs could be used.

This paper presents surface DBD operated in air at atmospheric pressure that could act as a source of ions used in synthesis of metallic nanoparticles. These reactive species could be introduced into an electrolyte filled with metallic precursor material, and act as a reducing agent, turning the dissociated metallic ions into atomic metal clusters. The charged species from DBD plasma are moved by the application of external electric field. It is possible to control the current density of introduced ions by regulation of the strength of this electric field. With a proper selection of surface active agents in the electrolyte and starting concentration of metallic salts, different sizes of monodisperse nanoparticles can be synthesized.

II. DISCHARGE MECHANISM

Capacitance of the dielectric limits the current in the electric circuit drastically, so that non-thermal discharges occur even at atmospheric pressure. As DBD is a type of non-equilibrium plasma, its constituent species are not at the thermodynamical equilibrium. Ions and neutrals are at nearly room temperature, while electrons have energies of over 10 eV (over 10⁵ K).

The discharge in this configuration occurs when charged particles are collected on the electrode and form a layer of high resistivity, which the electric current must pass through. The highly resistive layer does not allow the charge to decay at a desired rate, resulting in the build-up of an excess charge on the layer. When the voltage drop across the layer exceeds a critical value, an ultimate breakdown through the layer occurs. This breakdown is observed as fine discharge channels called microdischarges. The regular pulsed microdischarges are the result of the repeated charge accumulations and subsequent breakdown of the dielectric layer.

In the homogeneous field microdischarges will occur at each position within the gap simultaneously. As initial electrons, however, are statistically distributed along the electrode surface, avalanches will start at certain positions suppressing following ones in the surroundings by the field enhancement at the tip of the preceding avalanches. So, a multitude of isolated filamentary microdischarges well distributed on the discharge area will appear. Although even diffuse-homogeneous discharge modes can be observed at certain boundary conditions, the filamentary discharge mode is dominant at atmospheric pressure.

As the velocity of the charge carriers at breakdown field strength is rather high, the microdischarges are rapidly quenched by a growing counter-field, which results from charges collected on the surface of the dielectric. At further rise of voltage succeeding microdischarges will occur at locations apart of those of the preceding ones, at locations with enhanced local field strength. This happens up to voltage peak and again at decreasing voltage or at opposite polarity when the field strength in the gas gap reaches breakdown values again. These nanosecond microdischarges are shown in Fig. 1, where yellow plot represents voltage applied to the actuator, while current discharges are presented in green color.

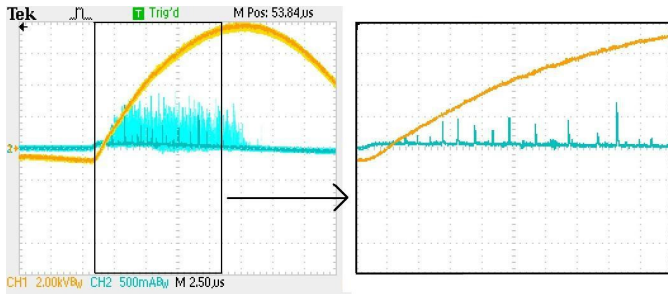


Figure 1. Shape of nanosecond discharges

III. SURFACE DBD PLASMA ACTUATORS

Four surface DBD plasma actuators were fabricated, with their characteristics provided in Table I. All DBD actuators have solid plate counter electrode, except the first which has interdigitated configuration (Fig. 2).

TABLE I. FABRICATED SURFACE DBD ACTUATORS

ID	Type	Dielectric	Area	Capacitance
1	Interdigitated	FR-4	12 cm ²	16 pF
2	Solid plate	FR-4	10 cm ²	20 pF
3	Solid plate	FR-4	33 cm ²	65 pF
4	Solid plate	Quartz	2 cm ²	3.5 pF

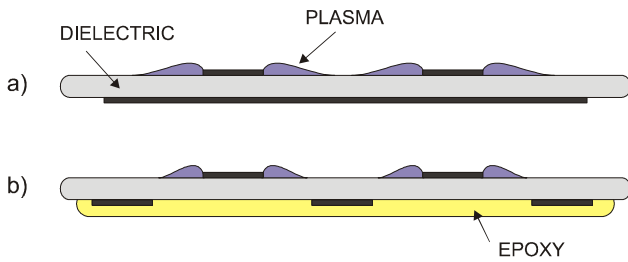


Figure 2. Schematic of surface DBD actuator: a) with solid plate counter electrode, b) interdigitated

The dielectric barrier has two main tasks: it quenches the microdischarges generating a fast pulsing system, and it distributes the microdischarges more or less uniformly over the discharge area. The choice of dielectric material strongly affects the operation of DBDs. It is important that dielectric has large dielectric strength (maximum electric field it can withstand) so that it can sustain application of high voltages. The following dielectrics were used: 1.5 mm thick copper laminated FR-4 plate ($\epsilon_r = 4.8$, $E_{\text{STRENGTH}} = 20$ kV/mm) and 1 mm thick quartz glass ($\epsilon_r = 3.8$, $E_{\text{STRENGTH}} = 25\text{-}40$ kV/mm). Fig. 3 shows capacitances of the actuators measured using HP4194A Impedance Analyzer and it can be seen that they are almost constant throughout the whole frequency range of operation.

Top (exposed) and bottom (counter) electrodes of interdigitated actuator have the minimum mutual overlap, which minimizes the capacitance of this actuator. It can be seen in Table I that the first actuator has the smallest capacitance per

area. Counter electrode of the interdigitated actuator has been covered with epoxy paste to improve stability (prevent creation of unwanted high-current sparks) and inhibit creation of plasma on the bottom side of the actuator.

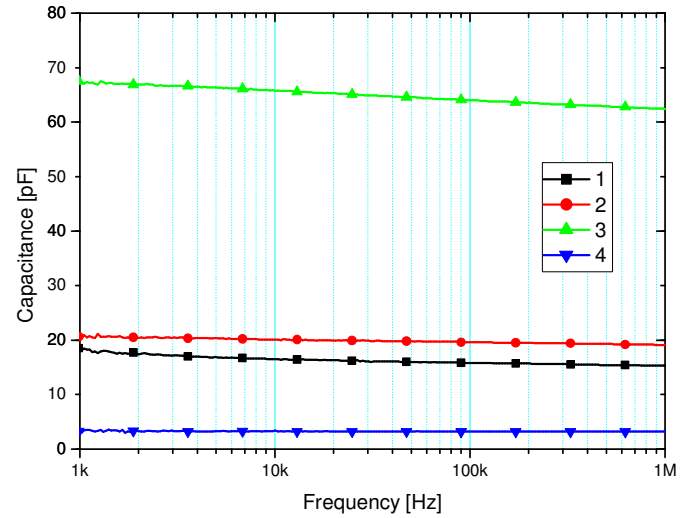


Figure 3. Capacitance characteristics of fabricated plasma actuators

IV. CHARACTERIZATION OF PLASMA ACTUATORS

A high voltage generator used to ignite plasma is based on a fly-back transformer powered by a 50 W chopping power source with adjustable amplitude and frequency. It has been set to operate in the frequency range from 1 kHz to 40 kHz. Maximum amplitude of delivered voltage is frequency dependant, and is in the range 5-8 kV. The voltage waveform at low frequencies consists of a large peak followed by small oscillations, while at frequencies over 25 kHz it enters sinusoidal regime. If the capacitance of connected actuator is larger, the waveform enters sinusoidal regime at lower frequencies.

A. Electrical Characterization

Electrical characterization was done using Tektronix TDS 2024B digital oscilloscope. For voltage measurement Tektronix P6015A HV probe was used, and current discharges that pass through dielectric are measured by Tektronix P6022 AC current probe. Due to very short current discharges and their random temporal occurrence, the option of 5 seconds persistence was enabled on the oscilloscope, thus the current discharges on all graphs are in fact all the discharges which occurred during 5 seconds of operation. This way statistically significant results are obtained. In all oscilloscope captures first channel presents voltage across the actuator (2 kV/div), and the second channel shows the current discharges through the actuator (500 mA/div). The time scale is 10 μ s/div.

Value of the voltage across the dielectric must be high enough in order that microdischarges could occur. Fig. 4 shows that 3 kV amplitude of applied voltage (10 kHz) is not high enough to ignite plasma on actuator #1, while at 6 kV and higher, many current discharges can be observed.



Figure 4. Current microdischarges through plasma actuator #1 operating at 10 kHz with applied voltage amplitudes of: a) 8 kV, b) 6 kV, c) 3 kV

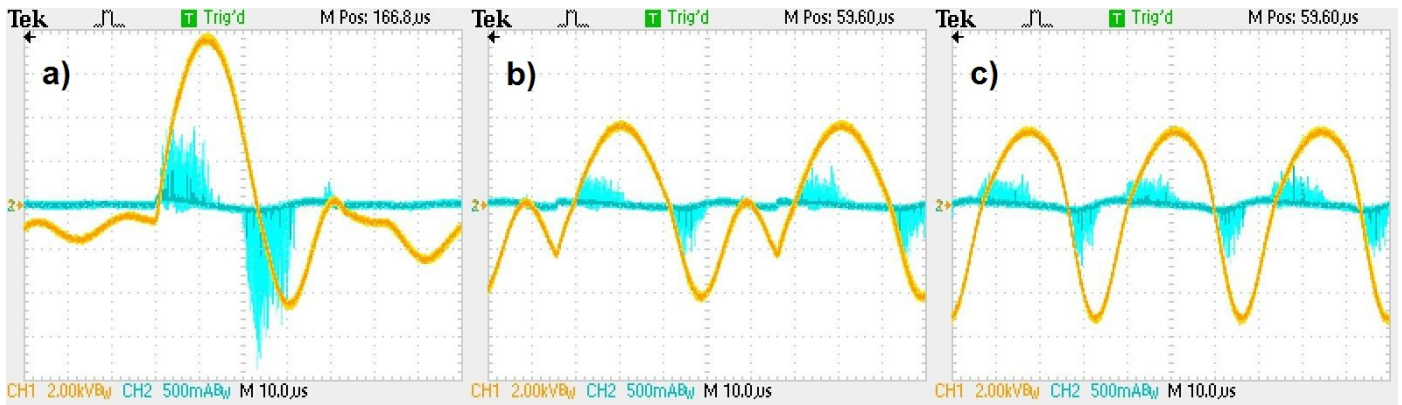


Figure 5. Current microdischarges through plasma actuator #1 at different driving frequencies: a) 10 kHz, b) 20 kHz, c) 30 kHz

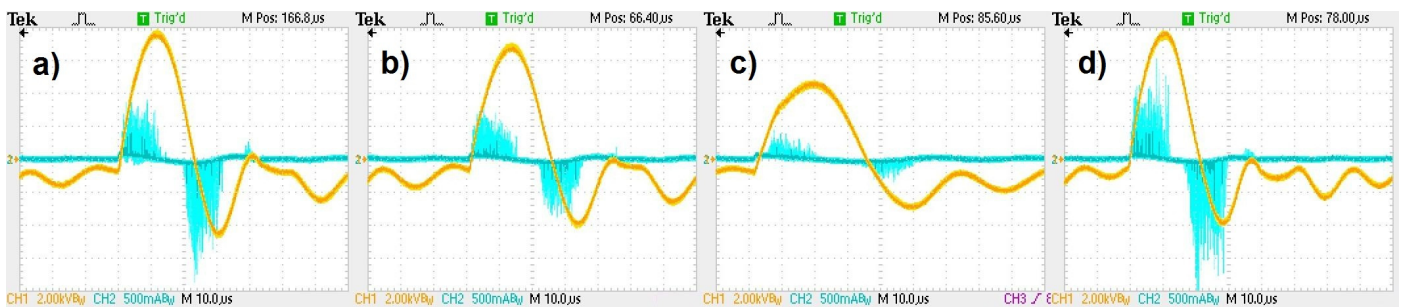


Figure 6. Voltage and current shapes of all plasma actuators operating on 10 kHz at maximum power, a) actuator #1, b) actuator #2, c) actuator #3, d) actuator #4

The change of frequency of the AC high voltage (HV) generator also impacts plasma generation, which is presented in Fig. 5. However, this is mostly due to frequency dependent efficiency of AC HV generator, which provides smaller peaks of HV at higher frequency for the same supplying power.

Finally, comparative results of all actuators at the same voltage supply are presented in Fig. 6. Plasma actuator #4 exhibits the most efficient discharges, closely followed by actuator #1. Actuator #2 gives smaller peaks due to losses in the dielectric. Large capacitance of actuator #3 influences the voltage shape by flattening its peak, which leads to poor discharge efficiency.

B. Thermal Characterization

During the operation, temperature of dielectric plate in the actuator rises. As the frequency of the applied voltage is in kilohertz range and its amplitude is several kilovolts, dielectric losses, which lead to heating, are not negligible. They can be reduced by change of geometry of the counter electrode. Actuator #1 with interdigitated electrodes emits less heat than actuator #2 of the same size with solid counter electrode. Both of the used surface materials have similar heat capacity. Specific heat of FR-4 is 600 kJ/kgK, while specific heat of quartz is 830 kJ/kgK.

Energetic electrons present another heating source. Although they are extracted from the plasma cloud and do not elevate its temperature, during the recombination they raise the

temperature of the active electrode due to electronic collisions. This heating can not be avoided. Heating curves of plasma actuators during 3 minutes of operation are presented in Fig. 7. It can be seen that the temperature rises rapidly during the first minute of operation, and after 2 minutes it almost settles. The low temperature of actuator #3 is the result of its large dielectric plate which acts as a heat sink.

Thermal images of plasma actuators after 2 minutes of operation on maximum power are obtained with ULIRvision TI160 IR camera and presented in Fig. 8. Maximum temperatures of actuators #1, #2, and #3 are reached in the dielectric, and their values are 82 °C, 105 °C, and 62 °C, respectively. Actuator #4 reaches its maximum temperature (180 °C) on the top electrode, while temperature of dielectric stays at 154 °C, which is still much larger than in the case of other actuators.

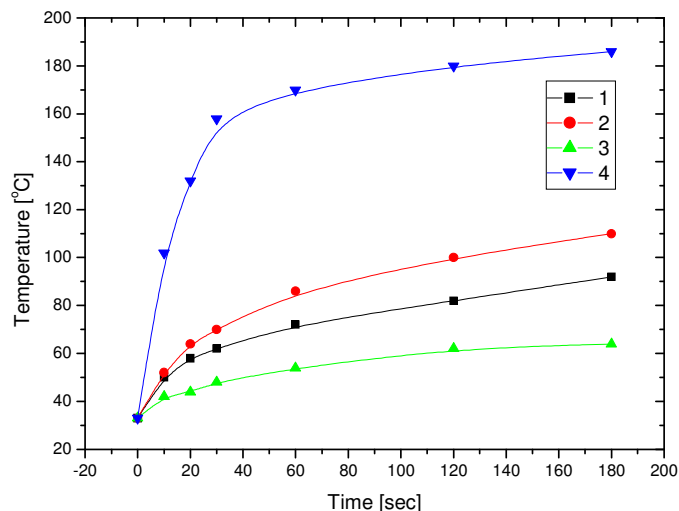


Figure 7. Heating curves of different plasma actuators during 3 minutes of operation at maximum power

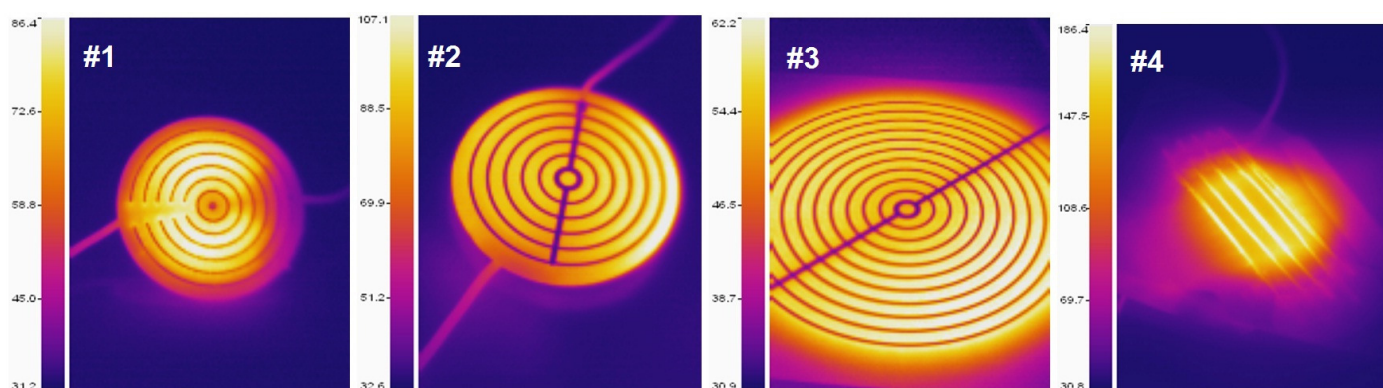


Figure 8. Thermal images of all fabricated plasma actuators after 2 minutes of operation

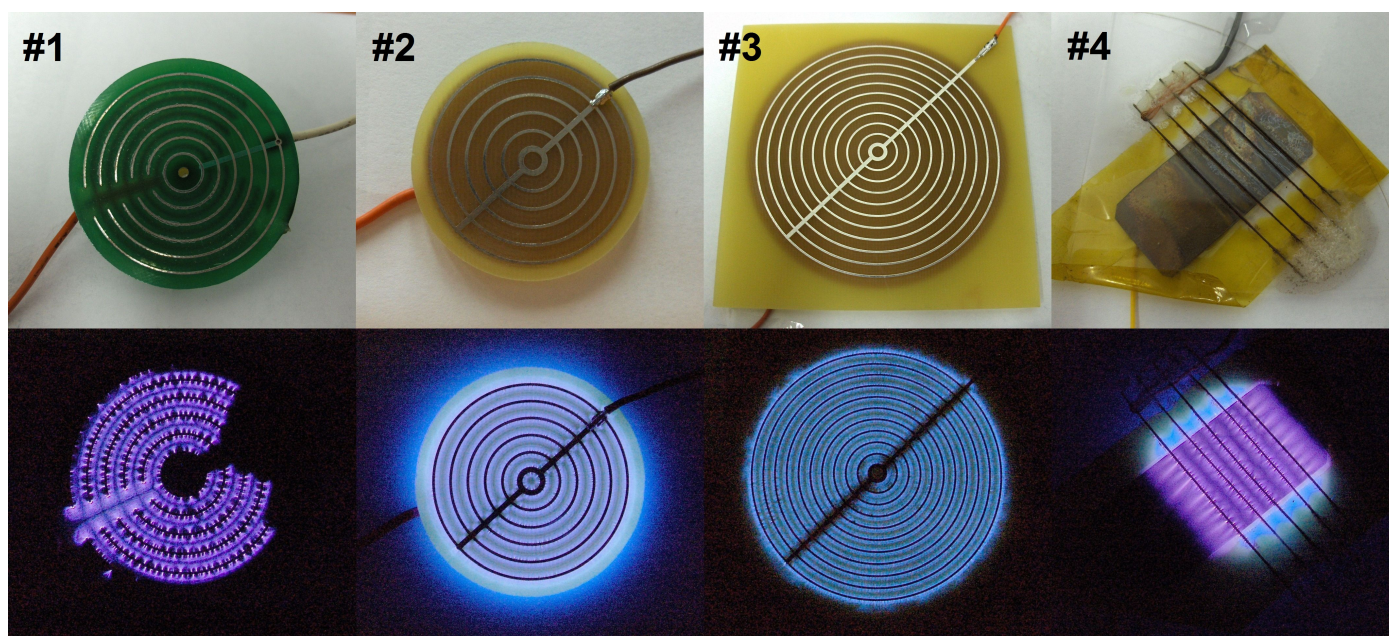


Figure 9. Comparative display of all fabricated plasma actuators with plasma off (up) and on (down)

C. Optical Characterization

Optical characterization of operating plasma actuators was done by digital camera with exposition value set to 4 seconds. The actuators in the off-state and operating on the 10 kHz are shown in Fig. 9. The intensity of emitted light corresponds to the thermal images of the actuators. Actuator #1 shows mostly filamented discharges. Actuators #2 and #3 exhibit the “underglow” produced by their counter electrodes, since they are not covered with epoxy resin. This effect is the most obvious on actuator #4, with transparent dielectric barrier.

Top electrodes on actuators #1, #2 and #3 are made using standard PCB fabrication process. Width of these copper lines is 0.5 mm and the distance between lines is 2.5 mm. Top electrode on actuator #4 is made of 0.3 mm thick steel wire, and the distance between the lines is 3 mm.

V. CONCLUSION

We compared electrical, thermal and optical characteristics of four plasma actuators made for the synthesis of metal nanoparticles. The fourth actuator with the quartz dielectric showed the best performances due to thin dielectric with very smooth surface, but it has serious thermal issues. This disadvantage could be solved by making an interdigitated DBD actuator with quartz dielectric.

Actuators with solid plate counter electrode and FR-4 dielectric show stable operation, but with less efficiency than the interdigitated actuator. Actuator #1 is being successfully used as a part of an apparatus for the synthesis of silver nanoparticles. It also exhibited a great stability during several hours of uninterrupted operation in the nanoparticle synthesis.

ACKNOWLEDGMENT

This work is partially supported by EC FP7 REGPOT project APOSTILLE, grant no. 256615 and also project TR32016.

REFERENCES

- [1] J. R. Roth “Industrial Plasma Engineering, vol. 2: Applications to nonthermal plasma processing”, IOP Publishing, 2001.
- [2] K. H. Becker, U. Kogelschatz, K. H. Schoenbach, and R. J. Barker, “Non-equilibrium air plasmas at atmospheric pressure”, IOP Publishing, 2005.
- [3] K. H. Becker, K. H. Schoenbach, and J. G. Eden “Microplasmas and applications”, J. Phys. D: Appl. Phys., vol. 39, pp. 55-70, 2006.
- [4] Fridman, A. Chirokov, and A. Gutsol “ Non-thermal atmospheric pressure discharges”, J. Phys. D: Appl. Phys., vol. 38, pp. 1-24, 2005.
- [5] T. Kaneko, K. Baba, and R. Hatakeyama, “Gas-liquid interfacial plasmas: basic properties and applications to nanomaterial synthesis”, Plasma Phys. Contr. F., vol. 51, 2009.
- [6] I. G. Koo, M. S. Lee, J. H. Shim, J. H. Ahn, and W. M. Lee, “Platinum nanoparticles prepared by a plasma-chemical reduction method”, J. Mater. Chem., vol. 5, pp. 4125-4128, 2005
- [7] J. Zou, Y. Zhang, and C. Liu “Reduction of supported noble-metal ions using glow discharge plasma”, Langmuir, vol. 22, pp. 11388-11394, 2006.
- [8] C. Richmonds, and R. M. Sankaran, “Plasma-liquid electrochemistry: Rapid synthesis of colloidal metal nanoparticles by microplasma reduction of aqueous cations”, Appl. Phys. Lett., vol. 93, 2008.
- [9] Z. Wei, C. Liu “Synthesis of monodisperse gold nanoparticles in ionic liquid by applying room temperature plasma”, Mater. Lett., vol. 65, pp. 353-355, 2011.
- [10] H. Furusho, K. Kitano, S. Hamaguchi and Y. Nagasaki “Preparation of stable water-dispersible PEGylated gold nanoparticles assisted by nonequilibrium atmospheric-pressure plasma jets”, Chem. Mater., vol. 21, pp. 3526-3535, 2009.
- [11] N. Kulbe, O. Hoeffft, A. Ulbrich, S. Z. El Abedin, S. Krischok, J. Janek, M. Poelleth, and F. Endres “Plasma electrochemistry in 1-butyl-3-methylimidazolium dicyanamide: Copper nanoparticles from CuCl and CuCl₂”, Plasma Process. Polym., vol. 8, pp. 32-37, 2011